ACS APPLIED NANO MATERIALS

www.acsanm.org

Letter

Facile Fabrication of Gold Nanorods@Polystyrenesulfonate Yolk–Shell Nanoparticles for Spaser Applications

Roman G. Parkhomenko* and Mato Knez

Cite This: ACS Appl. Nano Mater. 2022, 5, 4629–4633

Read Online

ACCESS | Metrics & More | Article Recommendations | Supporting Information

ABSTRACT: We present a method for producing gold nanorods surrounded by a hollow polymeric shell of polystyrenesulfonate and show that the cavities of such particles can be filled with various organic dyes. The approach consists of covering gold nanorods with silica, followed by its slow hydrolysis in an aqueous medium in the presence of the polymer thin layer permeable for dye molecules. The proposed method enables the yolk–shell nanoparticles to be obtained and loaded with organic dyes without a need to use thermal treatment and/or chemical etching, which makes it suitable for use in the creation of spasers.

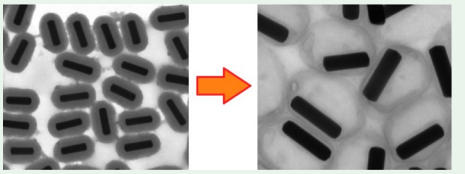

KEYWORDS: *yolk–shell, core–shell, gold nanoparticles, polystyrenesulfonate, spaser*

Despite the enormous amount of research done on gold nanoparticles (GNPs), they are still of tremendous interest for their unique optical, catalytic, and electronic properties, etc.[1,2] For example, many of the current rapid SARS-CoV-2 self-tests rely on GNPs, which results from their facile functionalization for biomedical applications.[3,4] The most recently explored application of gold nanoparticles is their utilization as a resonator in plasmonic nanolasers (spasers).[5,6] Here, GNPs are surrounded by a thin layer of an active medium whose emission band overlaps with the spectrum of localized surface plasmons of the GNP. For this purpose, colloidal core–shell spasing nanoparticles have been created, where molecules of an active medium are infiltrated into the mesoporous silica shell surrounding the gold core. The downside is that the amount of the dye involved in the spaser generation, and consequently the intensity of generation, is limited by the pore capacity of the silica shell. In contrast to the mesoporous silica, yolk–shell particles, due to their larger available volume, are outstanding alternative candidates for the spaser creation. Besides, such particles can also be used as nanoreactors or biological probes for cancer detection, which emphasizes their versatility.[7,8]

The currently dominant applied strategy to obtain yolk–shell particles relies on the removal of a sacrificial template.[9] This route can be described as a shell-by-shell deposition process where core–shell particles are covered with an additional outer shell of an organic or inorganic material. Subsequently the inner shell, which served as a template, is removed by dissolution with chemical agents or by heating, thereby forming yolk–shell particles. Silicon dioxide is the most common sacrificial template for yolk–shell particles of different types owing to its fabrication simplicity, nontoxicity, and chemical affinity to various core materials.[10] For example, space-confined synthetic approaches were used to obtain various types of yolk–shell particles.[11−14] Past studies have showed that different functional substances, such as therapeutic agents, can be incorporated into yolk–shell nanoparticles.[15,16] However, most of the current synthetic approaches involve multistep synthetic procedures, including thermal treatment and/or chemical etching. Furthermore, the loading of the hollow space with chemicals often requires additional processing steps which eventually lead to a low loading.[17−19] Thus, a straightforward and reproducible approach to fabricate yolk–shell nanoparticles is still a challenge and highly desired. In this work we present a facile method to obtain gold nanorod (GNR)-containing yolk–shell nanoparticles by the formation of a polystyrenesulfonate (PSS) shell with simultaneous hydrolysis of a previously grown sacrificial silica template in an aqueous medium. The resulting particles are extraordinarily stable in both polar and nonpolar solvents and exhibit a high loading capacity for organic dyes.

The GNRs were synthesized following the procedure described elsewhere with minor modifications by the reduction of chloroauric acid with 3-aminophenol in the presence of CTAB.[20] In the next step GNR@mesoporous silica core–shell structures (GNR@mSiO_2) were fabricated by adding tetraethoxysilane to the freshly synthesized GNR suspension (see details in the Supporting Information). The mesoporous silica layer, with a thickness of ∼35 nm, uniformly coats the surface of the GNR with open mesoporous channels pointing radially away from the gold core (Figure 1a, inset). These particles are positively charged (+35 mV), due to remaining

Received: March 4, 2022
Accepted: April 8, 2022
Published: April 12, 2022

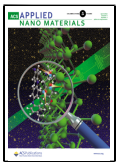

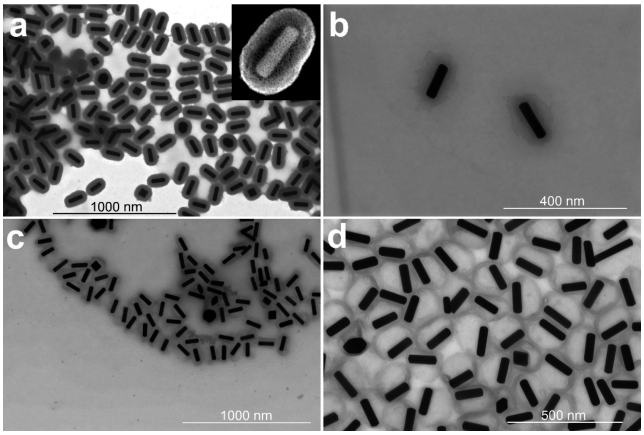

Figure 1. TEM images of GNR@mSiO$_2$@PSS particles after (a) 4 h of hydrolysis, (b) 24 h of hydrolysis, (c) 48 h of hydrolysis, and (d) final GNR@PSS particles.

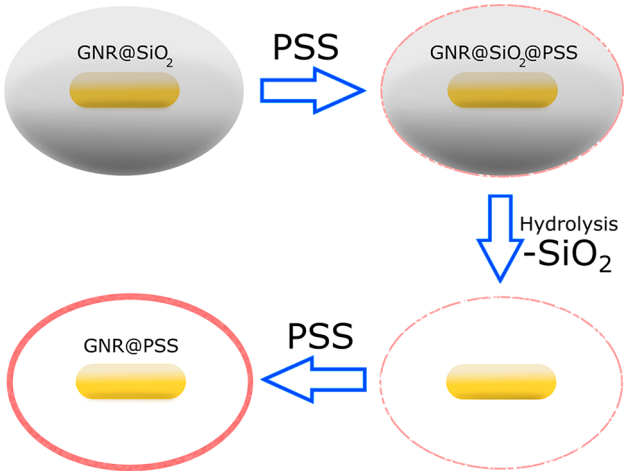

Figure 2. Scheme of GNR@PSS particles synthesis.

CTAB molecules, and do not undergo any visible morphological change even after several months of storage.

Then the particles were coated with a thin layer of PSS, a negatively charged polyelectrolyte which electrostatically interacts with the silica surface resulting in the GNR@mSiO$_2$@PSS particles formation. After solvent removal by centrifugation and addition of water, the sacrificial silica layer slowly hydrolyses and is completely removed within 48 h.[21] It is known that the synthesis of silica nanoparticles by sol−gel methods usually takes place through incomplete hydrolysis and polycondensation of organosilane precursors (e.g., TEOS). The presence of highly disordered and discontinuous Si−O−Si bonds results in the formation of amorphous SiO$_2$ structures. Such colloidal particles, when diluted in water, can undergo hydrolysis via breaking the Si−O−Si network and producing mainly orthosilicic acid Si(OH)$_4$ until an equilibrium is established.[22−24]

To understand the etching process in more detail and to monitor how the GNR@mSiO$_2$@PSS core−shell particles transform into yolk−shell structures, time-dependent TEM monitoring was conducted (Figure 1). As it can been seen in Figure 1a, within 4 h after centrifugation the particles still maintained their original shape and structure. At this stage we could not clearly observe the PSS layer on the surface, which is due to the low contrast difference between silica and the polymer. Twenty-four hours (Figure 1b) later the particles no longer had clear boundaries, likely due to the diffusion of silica hydrolysis products. After 48 h (Figure 1c), because most of the silica had been dissolved, a PSS layer with a thickness of several nanometers became visible (more detailed pictures are in Supporting Information Figure S1). It should be noted that the hydrolysis process was carried out at rest since intense mixing, heating, or sonification led to the collapse of the PSS shell. Afterward, to enlarge the shell thickness up to 15 nm (Figure 1d), more polymer was added and gently mixed for 8 h at room temperature, yielding stable GNR@PSS particles (a picture of low magnification is presented in Figure S2). The scheme of the entire process is depicted in Figure 2. When the first polymer portion is added, the PSS molecules electrostatically interact with the positively charged porous SiO$_2$ surface, forming a thin layer. The distance between the molecules is large enough and therefore porous enough for the products of silica hydrolysis, mainly Si(OH)$_4$, to pass through the layer. The interaction between neighboring polymer molecules is likely to be reinforced by Si(OH)$_4$ molecules situated between PSS chains, forming a network, which contributes to the stability of the shell. This hypothesis is indirectly confirmed by EDX (Figure S3), where the presence of silicon in the shell is visible. When more polymer is added, the PSS chains become embedded into the network or stacked on top of it, thereby densifying the shell. According to dynamic light scattering measurements, the yolk−shell particles are negatively charged (−42 ± 2 mV; Figure S4) with a hydrodynamic diameter of 140 nm, which is in good agreement with TEM data. When the particles are completely formed, they are stable in water, ethanol, THF, DMSO, and other solvents.

Figure 3a shows the UV−vis spectra of the samples studied. The absorption peak around 520 nm corresponds to the transverse surface plasmon band of the GNR; the absorption peak around 840 nm is ascribed to the longitudinal surface plasmon resonance band (LSPR). In comparison with the GNR, the LSPR band of GNR@mSiO$_2$ nanoparticles is red-shifted by about 21 nm (from 831 to 852 nm) due to the difference in the local dielectric constants of the surrounding medium. However, after the formation of GNR@PSS yolk−shell structures, the LSPR band blue-shifted from 852 to 840 nm, resulting from the removal of the mesoporous SiO$_2$ shell. Figure 3b shows the FTIR spectrum of the GNR@PSS particles (red curve), which is very similar to that of pure PSS (black curve). The broad peak in the frequency region of 3700−3000 cm^{-1} (OH stretching vibration) as well as the band in 1700−1570 cm^{-1} (H_2O scissoring vibration) result from residual water in the samples. The peaks at 2921 and 2850 cm^{-1} are attributed to the stretching vibration of methylene groups of the polymeric chain, and the bands at 1123 and 1008 cm^{-1} can be assigned to the in-plane skeleton and bending vibrations of the benzene ring. The peaks at 1183 and 1034 cm^{-1} are attributed to the antisymmetric and symmetric vibrations of SO_3 groups, respectively. Note that a decrease in the intensity of the 673 cm^{-1} band (S−O vibration) is likely related to the decreased polarity of the SO_3 groups associated with the positively charged remains of GNR@mSiO$_2$.[25] The XRD patterns of the GNR@PSS particles show three well-resolved diffraction peaks corresponding to the 111, 200, and 220 planes of face-centered cubic metal gold (PDF 4-784) with a good crystallinity (Figure S5). A characteristic halo at around 20−30°, corresponding to amorphous silica, was absent.

https://doi.org/10.1021/acsanm.2c00967
ACS Appl. Nano Mater. 2022, 5, 4629−4633

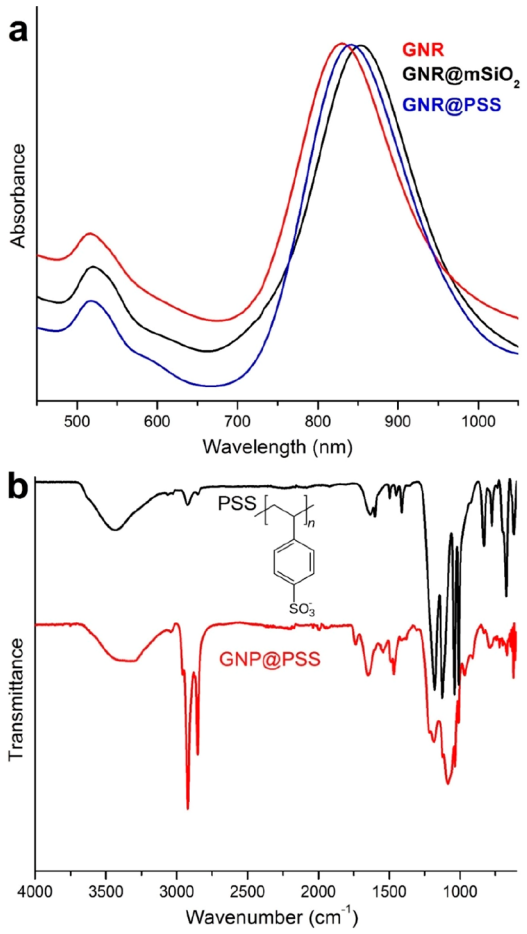

Figure 3. (a) UV−vis spectra of GNR, GNR@mSiO$_2$, and GNR@PSS particles. (b) FTIR spectra of GNR@PSS and pure PSS.

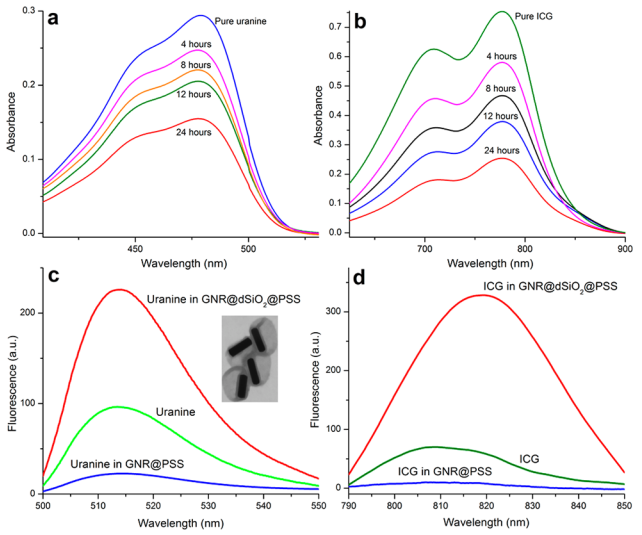

Figure 4. UV−vis absorption spectra (a, b) of original uranine (a) ICG and (b) aqueous solutions and the residual content of the dyes in the supernatant after interaction with GNR@PSS particles. Fluorescence emission spectra (c, d) of the uranine-loaded (c) and ICG-loaded (d) GNR@dSiO2@PSS yolk−shell particles.

Inspired by the developed synthetic approach, we elaborated a simple method to fill the yolk−shell particles with organic dyes.

Because the removal of the sacrificial silica layer was caried out in the presence of the initially thin PSS layer, we considered this layer to be largely permeable to various molecules. Therefore, we added uranine (fluorescein sodium salt) or indocyanine green (ICG) to the nanoparticles suspension 48 h after the start of the hydrolysis. To encapsulate the dye molecules within the yolk−shell particles, we added more polymer to the suspension at various time intervals. The loading capacity of the GNR@PSS particles was estimated differentially by UV−vis intensity measurements of the dye supernatants obtained after centrifugation at 488 nm (uranine) and 770 nm (ICG). We observed that the amount of the encapsulated dyes increases with time, as evidenced from a decrease in the intensity of the supernatant solutions. It reaches a maximum after 24 h and does not change afterward (Figure 4a,b). The results of our study show that up to 46% of uranine and 68% of ICG was captured by the GNR@PSS nanoparticles. We speculate that the difference in the loading capacity can be explained by the difference in polarity of the dye molecules. ICG molecules contain one pyrrolium group (positive charge) and two sulfonic groups (negative charge). In purified water (pH ∼ 5.5) the sulfonic groups are partially protonated, which makes the molecules relatively more positively charged. Uranine molecules do not have such positively charged groups, and, consequently, the negatively charged PSS surface attracts ICG molecules more readily while repelling the negatively charged uranine molecules. It should be noted, when the dyes were added to the stable particles whose polymer shell was formed, the loading capacity did not exceed 10% in both cases. The procedure described in the present work does not require the use of any etching agents, heating, or additional chemical functionalization of the nanoparticles, which makes it very attractive from the point of view of practical applications.

Panels c and d of Figure 4 show the emission spectra of the GNR@PSS particles filled with uranine and ICG at the maximum loading capacity. All of the emission spectra were measured at excitation wavelengths of 488 nm (uranine) and 775 nm (ICG). The fluorescence intensity of the uranine-/ICG-loaded GNR@PSS particles was lowered compared to the pure dye solutions of the same concentration. We assume that this fact is associated with the nonradiative energy transfer processes arising when a metallic surface is in direct contact with the fluorophore.[26,27] To avoid this effect, prior to obtaining mesoporous silica shell, the gold nanorods were covered with a thin layer of ordinary dense silica (GNR@dSiO$_2$), which does not undergo hydrolysis and retains its integrity within the entire synthesis process (Figure 4c, inset). According to the literature, to reach the maximum of fluorescent enhancement, the optimal thickness of such an initial shell should lie in the range between 7 and 15 nm.[28] In our experiments the shell thickness was ∼10 nm (Figure S6). In this case, the fluorescence enhancement factors were 2.3 (uranine) and 4.7 (ICG). The lower amplification factor of uranine can be explained by the lower overlapping between the transverse surface plasmon band of GNR and the absorption bands of the dye. Another possible explanation is that the fluorescence of molecules with a quantum yield close to unity can only be amplified via the excitation rate, while the emission of less efficient emitters can be enhanced via both the excitation rate and the increase of quantum efficiency.[29] The dye amount released from the particles after 24 h was ∼10%

https://doi.org/10.1021/acsanm.2c00967
ACS Appl. Nano Mater. 2022, 5, 4629−4633

for both fluorophores, and there was almost no release afterward.

In summary, we proposed a facile and reliable method to obtain GNR@PSS yolk−shell nanoparticles through the gradual formation of the polymer shell and simultaneous etching of sacrificial mesoporous silica. This approach makes it possible to charge the particles with organic dyes without using additional chemicals or etching agents. The particles have a high loading capacity, exceptional stability, and a great potential for spaser applications. They can also be used for other purposes such as the creation of biomedical probes, nanocontainers, and so on.

■ ASSOCIATED CONTENT

Supporting Information

The Supporting Information is available free of charge at https://pubs.acs.org/doi/10.1021/acsanm.2c00967.

Experimental section and additional supporting data such as TEM images, ζ-potential, XRD pattern, and EDX map (PDF)

■ AUTHOR INFORMATION

Corresponding Author

Roman G. Parkhomenko − *CIC NanoGUNE, E-20018 San Sebastian, Spain;* orcid.org/0000-0003-4226-1957; Email: r.parkhomenko@nanogune.eu

Author

Mato Knez − *CIC NanoGUNE, E-20018 San Sebastian, Spain; IKERBASQUE, Basque Foundation for Science, E-48009 Bilbao, Spain;* orcid.org/0000-0002-9850-1035

Complete contact information is available at: https://pubs.acs.org/10.1021/acsanm.2c00967

Funding

The European Union's Horizon 2020 research and innovation program under the Marie Sklodowska-Curie grant agreement No. 838845. The Maria de Maeztu Units of Excellence Programme: Grant Number CEX2020−001038-M. Spanish Ministry of Science and Innovation (MICINN) Grant Agreement No. PID2019−111065RB-I00.

Notes

The authors declare no competing financial interest.

■ ACKNOWLEDGMENTS

R.G.P. thanks the European Union's Horizon 2020 research and innovation programme under the Marie Sklodowska-Curie Grant Agreement No. 838845. M.K. is grateful for funding from the Maria de Maeztu Units of Excellence Programme: Grant No. CEX2020-001038-M. This work received funding through Grant No. PID2019-111065RB-I00, funded by MCIN/AEI/10.13039/501100011033 and by the "European Union".

■ ABBREVIATIONS

CTAB, cetyltrimethylammonium bromide
EDX, energy-dispersive X-ray spectroscopy
GNP, gold nanoparticles
ICG, indocyanine green
PSS, polystyrenesulfonate
TEM, transmission electron microscopy

■ REFERENCES

(1) Ishida, T.; Murayama, T.; Taketoshi, A.; Haruta, M. Importance of Size and Contact Structure of Gold Nanoparticles for the Genesis of Unique Catalytic Processes. *Chem. Rev.* **2020**, *120*, 464−525.

(2) Jeong, H.-H.; Choi, E.; Ellis, E.; Lee, T.-Ch. Recent advances in gold nanoparticles for biomedical applications: from hybrid structures to multi-functionality. *J. Mater. Chem. B* **2019**, *7*, 3480−3496.

(3) Huang, Ch.; Wen, T.; Shi, F.-J.; Zeng, X.-Y.; Jiao, Y.-J. Rapid Detection of IgM Antibodies against the SARS-CoV-2 Virus via Colloidal Gold Nanoparticle-Based Lateral-Flow Assay. *ACS Omega* **2020**, *5*, 12550−12556.

(4) Pramanik, A.; Gao, Y.; Patibandla, S.; Mitra, D.; McCandless, M. G.; Fassero, L. A.; Gates, K.; Tandon, R.; Chandra Ray, P. The rapid diagnosis and effective inhibition of coronavirus using spike antibody attached gold nanoparticles. *Nanoscale Adv.* **2021**, *3*, 1588−1596.

(5) Parkhomenko, R. G.; Kuchyanov, A. S.; Knez, M.; Stockman, M. I. Lasing Spaser in Photonic Crystals. *ACS Omega* **2021**, *6*, 4417−4422.

(6) Galanzha, E. I.; Weingold, R.; Nedosekin, D. A.; Sarimollaoglu, M.; Nolan, J.; Harrington, W.; Kuchyanov, A. S.; Parkhomenko, R. G.; Watanabe, F.; Nima, Z.; Biris, A.; Plekhanov, A. I.; Stockman, M. I.; Zharov, V. P. Spaser as a Biological Probe. *Nat. Commun.* **2017**, *8*, 15528.

(7) Fan, L.; Xu, X.; Zhu, Ch.; Han, J.; Gao, L.; Xi, J.; Guo, R. Tumor Catalytic-Photothermal Therapy with Yolk-Shell Gold@Carbon Nanozymes. *ACS Appl. Mater. Interfaces* **2018**, *10*, 4502−4511.

(8) Lin, F.; Doong, R. Catalytic Nanoreactors of Au@Fe_3O_4 Yolk-Shell Nanostructures with Various Au Sizes for Efficient Nitroarenes Reduction. *J. Phys. Chem. C* **2017**, *121*, 7844−7853.

(9) El-Toni, A. M.; Habila, M. A.; Labis, J. P.; ALOthman, Z. A.; Alhoshan, M.; Elzatahry, A. A.; Zhang, F. Design, synthesis and applications of core−shell, hollow core, and nanorattle multifunctional nanostructures. *Nanoscale* **2016**, *8*, 2510−2531.

(10) Purbia, R.; Paria, S. Yolk/shell nanoparticles: classifications, synthesis, properties, and applications. *Nanoscale* **2015**, *7*, 19789−19873.

(11) Lu, X.; Liu, A.; Zhang, Y.; Liu, S. Space-confined synthesis of yolk−shell structured Co_3O_4/nitrogen-doped carbon nanocomposites with hollow mesoporous carbon nanocages as advanced functional anodes for lithium-ion batteries. *ACS Appl. Energy Mater.* **2020**, *3*, 11153−11163.

(12) Wang, B.; Ye, Y.; Xu, L.; Quan, Y.; Wei, W.; Zhu, W.; Li, H.; Xia, J. Space-confined yolk-shell construction of Fe_3O_4 nanoparticles inside N-doped hollow mesoporous carbon spheres as bifunctional electrocatalysts for long-term rechargeable zinc-air batteries. *Adv. Funct. Mater.* **2020**, *30*, 2005834.

(13) Xinxing, S.; Shuangke, L.; Weiwei, S.; Yujie, L.; Danqin, W.; Qingpeng, G.; Xiaobin, H.; Jing, X.; Chunman, Z. Nano-confined synthesis of multi yolk-shell Co-NC@N-HCSs hybrid as sulfur host for high performance lithium-sulfur batteries. *Electrochim. Acta* **2021**, *398*, 139302.

(14) Mirbagheri, R.; Elhamifar, D.; Shaker, M. Yolk-shell structured magnetic mesoporous silica: A novel and highly efficient adsorbent for removal of methylene blue. *Sci. Rep.* **2021**, *11*, 23259.

(15) Zhang, Ch.; Li, Y.; Hu, Y.; Peng, Y.; Ahmad, Z.; Li, J.-S.; Chang, M.-W. Porous yolk−shell particle engineering via nonsolvent-assisted trineedle coaxial electrospraying for burn-related wound healing. *ACS Appl. Mater. Interfaces* **2019**, *11*, 7823−7835.

(16) Saran, K.; Shi, P.; Ranjan, S.; Goh, J. C. H.; Zhang, Y. A moldable putty containing silk fibroin yolk shell particles for improved hemostasis and bone repair. *Adv. Healthcare Mater.* **2015**, *4*, 432−445.

(17) Li, G.; Chen, Y.; Zhang, L.; Zhang, M.; Li, S.; Li, L.; Wang, T.; Wang, Ch. Facile Approach to Synthesize Gold Nanorod@Polyacrylic Acid/Calcium Phosphate Yolk−Shell Nanoparticles for Dual-Mode Imaging and pH/NIR-Responsive Drug Delivery. *Nano-Micro Lett.* **2018**, *10*, 7.

(18) Xing, S.; Tan, L. H.; Chen, T.; Yang, Y.; Chen, H. Facile fabrication of triple-layer (Au@Ag)@polypyrrole core−shell and

(Au@H_2O)@polypyrrole yolk−shell nanostructures. *Chem. Commun.* **2009**, 1653−1654.
(19) Watanabe, K.; Welling, T. A. J.; Sadighikia, S.; Ishii, H.; Imhof, A.; van Huis, M. A.; van Blaaderen, A.; Nagao, D. Compartmentalization of gold nanoparticle clusters in hollow silica spheres and their assembly induced by an external electric field. *J. Colloid Interface Sci.* **2020**, *566*, 202−210.
(20) Wu, Z.; Liang, Y.; Cao, L.; Guo, Q.; Jiang, S.; Mao, F.; Sheng, J.; Xiao, Q. High-yield synthesis of monodisperse gold nanorods with a tunable plasmon wavelength using 3-aminophenol as the reducing agent. *Nanoscale* **2019**, *11*, 22890−22898.
(21) Yamada, H.; Urata, C.; Aoyama, Y.; Osada, S.; Yamauchi, Y.; Kuroda, K. Preparation of Colloidal Mesoporous Silica Nanoparticles with Different Diameters and Their Unique Degradation Behavior in Static Aqueous Systems. *Chem. Mater.* **2012**, *24*, 1462−1471.
(22) Hench, L. L.; West, J. K. The sol-gel process. *Chem. Rev.* **1990**, *90*, 33−72.
(23) Alexander, G. B.; Heston, W. M.; Iler, R. K. The solubility of amorphous silica in water. *J. Phys. Chem.* **1954**, *58*, 453−455.
(24) Kato, K.; Kitano, Y. J. Solubility and dissolution rate of amorphous silica in distilled and sea water at 20 °C. *Oceanogr. Soc. Jpn.* **1968**, *24*, 147−152.
(25) Yang, J. Ch.; Jablonsky, M. J.; Mays, J. W. NMR and FT-IR studies of sulfonated styrene-based homopolymers and copolymers. *Polymer* **2002**, *43*, 5125−5132.
(26) Anger, P.; Bharadwaj, P.; Novotny, L. Enhancement and Quenching of Single-Molecule Fluorescence Phys. *Rev. Lett.* **2006**, *96*, 113002−113006.
(27) Chen, H.; Ming, T.; Zhao, L.; Wang, F.; Sun, L. D.; Wang, J.; Yan, C. H. Plasmon-molecule interactions. *Nano Today* **2010**, *5*, 494−505.
(28) Zhang, B.; Wei, L.; Chu, Z. Development of indocyanine green loaded Au@Silica core shell nanoparticles for plasmonic enhanced light triggered therapy. *J. Photochem. Photobiol. A* **2019**, *375*, 244−251.
(29) Bharadwaj, P.; Deutsch, B.; Novotny, L. Optical Antennas. *Adv. Opt. Photon.* **2009**, *1*, 438−483.

https://doi.org/10.1021/acsanm.2c00967
ACS Appl. Nano Mater. 2022, 5, 4629−4633